RSC Advances

PAPER

View Article Online
View Journal | View Issue

Cite this: *RSC Adv.*, 2024, **14**, 3698

Evaluation of sustained drug release performance and osteoinduction of magnetron-sputtered tantalum-coated titanium dioxide nanotubes

Jing Zhan,[a] Li Li,[a] Lili Yao,[b] Zheng Cao,[a] Weiwei Lou,[c] Jianying Zhang,[d] Jinsong Liu*[b] and Litao Yao*[a]

Modifying the drug-release capacity of titanium implants is essential for maintaining their long-term functioning. Titanium dioxide nanotube (TNT) arrays, owing to their drug release capacity, are commonly used in the biomaterial sphere. Their unique half open structure and arrangement in rows increase the drug release capacity. However, their rapid drug release ability not only reduces drug efficiency but also produces excessive local and systemic deposition of antibiotics. In this study, we designed a tantalum-coated TNT system for drug-release optimization. A decreased nanotube size caused by the tantalum nanocoating was observed through SEM and analyzed (TNT: 110 nm, TNT-Ta1: 80 nm, TNT-Ta3: 40 nm, TNT-Ta5: 20 nm, TNT-Ta7: <5 nm). XPS analysis revealed the distribution of the chemical components, especially that of the tantalum element. *In vitro* experiments showed that the tantalum nanocoating enhanced cell proliferation; in particular, TNT-Ta5 possessed the best cell viability (about 1.18 of TNT groups at 7d). It also showed that the tantalum nanocoating had a positive effect on osteogenesis (especially TNT-Ta5 and TNT-Ta7). Additionally, hydrophilic/hydrophobic drug (vancomycin/raloxifene) release results indicated that the TNT-Ta5 group possessed the most desirable sustained release capacity. Moreover, in this drug release system, the hydrophobic drug showed more sustained release capacity than the hydrophilic drug (vancomycin: sustained release for more than 48 h, raloxifene: sustained release for more than 168 h). More importantly, TNT-Ta5 is proved to be an appropriate drug release system, which possesses cytocompatibility, osteogenic capacity, and sustained drug release capacity.

Received 22nd December 2023
Accepted 5th January 2024

DOI: 10.1039/d3ra08769g

rsc.li/rsc-advances

1. Introduction

Titanium implants are widely applied in implantology owing to their excellent advantages such as good corrosion resistance, plasticity, and biocompatibility.[1–4] However, the antibacterial scarcity, poor osteo-induction ability, and potential allergic reaction of titanium implants may cause postoperative complications, thus, leading to premature implant loss.[3,5–7] Moreover, titanium-based implants can be easily modified by physical, chemical, and biological techniques.[8–10] In addition, with these surface modifications, both surface energy and osteogenesis could be promoted.[11] Among these techniques, the combination of drugs and implants is an effective method to enhance the pro-osteogenic and antibacterial activities.[12–14] Titanium dioxide nanotube arrays (TNTs) have been developed as an excellent drug container, which have the advantages of neat arrangement, controllable dimeter, high surface-to-volume ratio, and excellent biocompatibility.[15] Previous studies have proposed to prepare TNTs on medical implants as a drug release platform for clinical application.[16] Moreover, TNTs with drug loading properties, biocompatibility, and pro-osteogenic promotion ability have attracted much interest,[17,18] whereas rapid drug release caused by the large and straight diameter of TNTs would compromise their application.[17,19] Therefore, effective techniques are urgently needed to control drug release from TNTs, promoting their biological properties and avoiding excessive local drug concentration.

Numerous methods have been developed to optimize the drug release property of TNTs.[20–22] For instance, a layer-by-layer (LBL) self-assembly method was applied to slow down the drug release rate.[23] However, the LBL formed by electrostatic interactions between polycations and polyanions was easy to be detached.[23] Moreover, a super-hydrophobic titanium dioxide nanotube (S-TNT) array drug delivery system was investigated to

[a]*Department of Dentistry, Sir Run Run Shaw Hospital, School of Medicine, Zhejiang University, 3# Qingchun East Road, Shangcheng District, Hangzhou 310058, Zhejiang, China. E-mail: 3320080@zju.edu.cn*

[b]*School and Hospital of Stomatology, Wenzhou Medical University, 268# Xueyuan West Road, Lucheng District, Wenzhou, Zhejiang, China. E-mail: jinsong0719@wmu.edu.cn*

[c]*Department of Stomatology, The First Affiliated Hospital, College of Medicine, Zhejiang University, Hangzhou 310003, China*

[d]*International Healthcare Center, Sir Run Run Shaw Hospital, School of Medicine, Zhejiang University, Hangzhou 310058, China*

control drug release, while the osteogenic activity was still inadequate.[24] Compared to polymer coating techniques, functional metal/metal oxide coating methods possess advantages of simplicity, anti-corrosion properties, and high stability.[25–27] Therefore, controlling drug release from TNTs *via* metal/metal oxide coating is an effective method to achieve sustained drug release.

Based on the purpose of fabricating a drug release system by metal/metal oxide coating, the question still remained whether the narrowed outer diameter of nanotube could decrease the drug release rate and prolong the drug release duration. A previous study had covered the titanium dioxide nanotube array with ZnO and Sr to narrow the outer diameter of TNTs and enhance the osteogenic property, whereas the absence of drug release test failed to prove the function of drug release property.[15] Our previous study coated Ga_2O_3 nanocoating on TNTs by magnetron sputtering to endow the titanium implant with antibacterial and osteogenic property, proving that Ga_2O_3-coated TNTs was a promising drug release system.[28] However, Ga_2O_3 nano-coating was strictly dose-dependent and thus too thin to retard the drug releasing rate. Compared with Ga_2O_3, tantalum possessed excellent mechanical property and pro-osteogenic activity, which was conducive to osteointegration.[29] Moreover, the ideal porosity, modulus of elasticity, and coefficient of friction made it easy to reduce the stress shielding effectively.[30,31] Therefore, we deposited a tantalum nanocoating on TNTs in this study to narrow the orifice diameter of the nanotube by magnetron sputtering to fabricate a tantalum modified drug release system. Afterward, the hydrophilic/hydrophobic drug (vancomycin/raloxifene) was loaded as the model drug to evaluate the drug release property, and *in vitro* experiments were applied to evaluate the osteo-inductive property. We speculated that the covering of a suitable tantalum nanocoating could form a desirable drug delivery system, which could realize controllable drug release and osteogenic differentiation promotion. Two issues were intended to be solved in this study as follows: (1) selecting the objective group with sustained drug release property and excellent osteogenic ability. (2) Evaluating the biocompatibility, pro-osteogenic property, and drug release performance of the tantalum-modified drug release system by *in vitro* experiment.

2. Materials and methods

2.1 Materials

Titanium foils (thickness: 0.2 mm, length: 10 mm, width: 10 mm) were purchased from Northwest Institute (Xi'an, China) and washed with acetone, ethanol, and distilled water for 10 min before the experiment. Ammonium fluoride and glycerin were purchased from Aladdin Biotech (Shanghai, China). The hydrophilic drug (vancomycin) and hydrophobic drug (raloxifene) were purchased from Sigma Chemical. FITC-labeled phalloidin, MTT solution, dihydrochloride (DAPI), bicinchoninic acid kit (BCA), alkaline phosphatase (ALP), and alizarin red staining kit were purchased from Beyotime Biotechnology Co. (Shanghai, China). Tantalum target materials were supplied by ZhongNuo Advanced Materials Technology Co. (Beijing, China).

2.2 Sample preparation

The anodization procedure was conducted according to our previous study. In short, the electrolyte containing 50 wt% deionized water, 10 wt% ammonium fluoride, and 50 wt% glycerin was prepared. The pretreated pure titanium sheet (anode) and the platinum foils (cathode) were kept a distance of 10 mm and immersed in the electrolyte for anodization. The anodization parameters were set as follows: the direct current (DC) potential of 30 V for 1.5 h at 30 °C. After reaction, the anodized samples were taken out and ultrasonically cleaned with acetone, ethanol, and deionized water for 5 min. Finally, these samples were dried and stored in a vacuum device.

2.3 Magnetron sputtering of tantalum

The tantalum nanocoating was deposited onto TNTs *via* DC magnetron sputtering machine (VTC-600-2HD, Kejing Auto-Instrument Co., Shenyang, China). The prepared TNTs were placed on the rotating stage and 99.9% high purity tantalum target was used for magnetron sputtering. The specific parameters of magnetron sputtering were as follows: the power, voltage, and gas pressure were kept the same, while the sputtering durations was set as 1 min, 3 min, 5 min, and 7 min and denoted as TNT-Ta1, TNT-Ta3, TNT-Ta5, and TNT-Ta7, respectively. The specific parameters of magnetron sputtering are illustrated in Table 1. Therefore, the groups involved in this study were Ti, TNT, TNT-Ta1, TNT-Ta3, TNT-Ta5, and TNT-Ta7.

2.4 Surface characterization

Field emission scanning electron microscopy was used to detect the surface structure of different samples (FESEM, Nova NanoSEM200, FEI Co., USA), and the diameter of TNTs was analyzed by IPwin60. The chemical composition of Ti, TNT, TNT-Ta1, TNT-Ta3, TNT-Ta5, and TNT-Ta7 was detected *via* X-ray photoelectron spectroscopy (XPS, K-alpha, Thermo, USA), and the amount of Ta element was measured by XPS quantitative analysis. The hydrophilicity of the surface was detected by a water contact angle system (Model 200, Future Scientific, China). The crystal structure was accessed by X-ray diffraction (XRD, Philips X'Pert Pro). Four samples in each group were applied for water contact angle measurement. In short, 5 μL distilled water was dropped on the sample surface for 15 s at room temperature before imaging. Finally, water contact angle analysis (WCA, SL200B, Solon) was performed to evaluate the hydrophilic property. The average roughness of different substrates (6 samples/group) was detected in the examination

Table 1 The parameters of magnetron sputtering for the deposition of tantalum (Ta)

Variable factors	Ta1	Ta3	Ta5	Ta7
Power (watt)	100	100	100	100
Sputtering rate (nm s^{-1})	1	1	1	1
Base pressure (Pa)	5×10^{-4}	5×10^{-4}	5×10^{-4}	5×10^{-4}
Working pressure (Pa)	0.5	0.5	0.5	0.5
Time (min)	1	3	5	7

range (10 μm × 10 μm) by atomic force microscopy (AFM, Veeco Co, USA). In this way, roughness characterization including 3D images, mean roughness (Sa), and RMS roughness (Sq) of different substrates was acquired. Among them, Sa reflected the arithmetic average deviations of the profile height from the mean surface, and Sq indicated the root mean square average of the profile height deviations from the mean surface.

2.5 Drug release test

Vancomycin solution (1 mg mL^{-1}, 10 mL) and raloxifene solution (1 mg mL^{-1}, 10 mL) were prepared at room temperature. The drug-loaded samples were prepared by immersing in two solutions with 2 h of shaking. Therefore, the drug would be fully loaded into the nano-tube arrays of TNTs in this way. Afterward, each group of samples was put into 10 mL deionized water for 1 min to remove the residual solution, which was dried with nitrogen. Next, the samples were immersed in PBS solution (pH 7.4) at 37 °C for solution collection.

For the vancomycin-loaded samples, the immersion solution (0.5 mL) was collected and replaced with fresh PBS at the immersing duration of 12, 24, 36, 48, 60, and 72 h.

As for the raloxifene-loaded samples, the immersion solution (0.5 mL) was collected and replaced with fresh PBS at the incubation time points of 24, 48, 72, 96, 120, 144, and 168 h. The amount of vancomycin/raloxifene released into PBS was measured *via* a Nanodrop 2000 instrument at a wavelength of 280 nm.

2.6 *In vitro* cell evaluation

2.6.1 Cell culture. The MC3T3-E1 cells, purchased from ATCC (Chinese Academy of Science, China), were cultured in α-MEM medium containing 1% penicillin/streptomycin (Gibco) and 10% fetal bovine serum (FBS; Gibco) at 37 °C under 5% CO_2 humid culture condition. The culture medium was renewed every other day. Furthermore, trypsin–EDTA solution (0.25% trypsin, 1 Mm EDTA; Gibco) was added for cell detachment when the cell density reached 90% confluency. Finally, centrifugation at 1000 rpm was carried out for 5 min, and the culture medium was readded after discarding the supernatant liquid. Before cell seeding, all the specimens were sterilized with 75% ethanol and UV irradiation for 30 min and then rinsed with phosphate-buffered saline (PBS; Gibco) thrice. In order to prevent the effects of ethanol on the drugs, the sterilized samples (TNT and TNT-Ta) were used for drug loading, which was conducted in a sterile environment.

2.6.2 Cell viability. In this experiment, the thiazole blue (MTT) colorimetric method was used to detect the cell proliferation quantitively. The cell suspension was seeded on different specimens in 24-well plates with a cell density of 1×10^4 cm^{-2} and incubated for 4 and 7 days. The detection was conducted after 4 days and 7 days of cell culture. 50 μL MTT (5 mg mL^{-1}) was added into the culture medium in the dark condition and incubated at 37 °C for 4 h. Next, 1000 μL DMSO was added to each well to dissolve the formazan crystals, of which 200 μL was transferred to a 96-well plate, and the absorbance was read at a wavelength of 490 nm using a spectrophotometric microplate reader (Bio-Rad 680, USA).

2.6.3 Early adhesion and morphology of cells. Immunofluorescence staining was performed to detect the cell morphology. After 2 days of incubation of MC3T3-E1(seeding density: 8000 per cm^2), the Mc3T3-E1 cells were washed thrice with PBS and fixed with 4% paraformaldehyde for 1 h. Afterward, the cell membrane was perforated with 0.2% TritonX-100, whose cytoskeleton was stained with FITC-labeled phalloidin for 30 min, and the nucleus was stained with DAPI for 15 min. The treated specimens were then washed thrice with PBS and observed using a fluorescence microscope from five directions.

As for early adhesion, we used sterilized PBS to remove the impurities after 0.5 and 2 h of cell incubation (seeding density: 10 000 per cm^2). Next, 0.2% TritonX-100 was used to punch after cell fixation with 4% paraformaldehyde for 1 h. Afterward, the cytoskeleton was stained with FITC-labeled phalloidin for 30 min, and the nucleus was stained with DAPI for 15 min. The treated specimens were then washed thrice with PBS and observed using a fluorescence microscope from five directions. The experiment was repeated three times.

2.6.4 ALP activity. As for ALP activity detection, the MC3T3-E1 cells in different samples were lysed by 1% TritonX-100 for 50 min after osteogenic induction for 7 and 14 days. Then, the lysate was measured by ALP assay kit (Nanjing Jiancheng Bioengineering Institute, China) and BCA protein assay kit (Beyotime, China). 30 μL cell lysis solution on each well was detected by the ALP kit, and the absorbance was read at a wavelength of 520 nm by a microplate reader (Bio-Rad 680, USA). Meanwhile, 20 μL cell lysis solution on each well was detected by the BCA protein assay kit, and the absorbance was read at a wavelength of 562 nm by a microplate reader (Bio-Rad 680, USA). Finally, the ALP activity was normalized by protein concentration and expressed in nanomoles of *p*-nitrophenol produced per milligram of protein per minute.

2.6.5 Mineralization. The contents of matrix mineralization were measured by alizarin red staining, according to a previous study.[32] The samples were collected after being cultured with osteogenic induction medium (α-MEM, 100 nM dexamethasone, 10 mM beta-glycerol phosphate, and 50 μg mL^{-1} ascorbic acid) for 14 days in an incubator. Next, the samples were immersed in 4% paraformaldehyde for 60 min. The residual liquid on the samples was washed with PBS 5 times. Samples were then immersed in Alizarin Red S (pH 4.2) for 80 min. Afterward, we used deionized water to eliminate the extra staining until the impurities were removed thoroughly. Accordingly, the mineralized calcium nodules were dissolved by 10% cetylpyridinium chloride (Sigma, USA) and 200 μL solution of each well was absorbed into a 96-well plate and analyzed by a microplate reader (Bio-Rad 680, USA) at the wavelength of 540 nm.

2.6.6 Quantitative real-time PCR. The osteogenesis-related genes expression was determined by RT-qPCR after 14 days of cell culture. Five osteogenesis relevant primers, namely, type-1 collagen (COL-1), alkaline phosphatase (ALP), osteopontin (OPN), osteocalcin (OCN), and Runx2, were selected for quantitative reverse transcription quantitative real time polymerase

chain reaction (qRT-PCR). The total RNA was obtained using RNA extraction kit (Thermo, USA), whose concentration was detected by a Nanodrop spectrophotometer (Thermo, USA). 20 μL RNA from each group was reverse transcribed into synthesized cDNA using the PrimeScript™ RT Master Mix (Perfect Real Time, Takara, China). The TB Green® Premix Ex Taq™ kit (Takara Biotechnology, Japan) and qRT-PCR analysis device (Applied Biosystem 7500) were applied for detection. The sequences of different primers we used in this step are displayed in Table 2, and GAPDH was used as the reference gene.

2.7 Statistical analysis

All data in this study were expressed as means ± standard deviation (SD). The statistical analysis was performed through Student's *t*-test and one-way analysis of variance (ANOVA) using Origin Pro at 95% and 99% confidence levels.

3. Results and discussion

3.1 Surface characterization

The surface structure of different specimens was characterized by FE-SEM (Fig. 1A). The Ti samples showed smooth surface with no obvious impurities, while an ordered TiO_2 nanotubes possessed an average outer diameter of 110 nm (Fig. 1A and C). After tantalum nanocoating deposition, the diameter of TiO_2 nanotubes was decreased with the extension of sputtering duration (TNT-Ta1: 80 nm; TNT-Ta3: 40 nm; TNT-Ta5: 20 nm; TNT-Ta7 <5 nm). Moreover, FE-SEM showed that the deposited tantalum nanocoating was dense and uniformly distributed over the TNTs. The procedure of magnetron sputtering had advantages of uniform distribution, dense and controllable layer, low temperature requirement, and high bind strength.[33] Zeliang Ding *et al.* prepared multilayer Cu-mTa_2O_5 composite coatings on Ti6Al4V alloy for biomedical applications by magnetron sputtering, realizing an enhanced anticorrosion performance and superior antibacterial effects.[34] As for surface topography, previous studies proved that TNTs with large diameter (110–150 nm) were beneficial for osteogenic differentiation, while a small diameter (15–70 nm) was conducive to the cell proliferation of MC3T3-E1.[35] Among them, TNTs with diameter of 15 nm possessed the highest cell biocompatibility.[17] Moreover, a previous study fabricated TNTs with a diameter of 25 nm and 80 nm on the titanium surface to evaluate the biological property of mesenchymal stem cells (BMSCs). The results indicated that TNTs with 25 nm size had significantly higher osteogenic gene related expression than those with 80 nm size.[36] However, previous studies showed that TiO_2 with pore diameter of 70 nm exhibited promising osteo-induction property, which was mainly attributed to the favorable hydrophilicity, protein adsorption ability, and pro-osteogenic functions caused by the "capillary" of nanotube topography and hydroxyl groups.[37,38] Nevertheless, the structure with small nanotube diameter was conducive to chondrogenic differentiation. The surface structure with small nanotube diameter was found to impede the endochondral ossification.[39] Therefore, TNTs with different sizes of nanotube diameter possessed different biological functions under different conditions. Though the most suitable nanotube diameter of TNTs has not been standardized yet, the biological response of different substrates was the joint effect of tantalum and surface physical properties. In this study, the tantalum nanocoating was applied to adjust the diameter of the nanotube to optimize the drug release property. TNTs with decreased nanotube diameter (TNT-Ta1: 80 nm; TNT-Ta3: 40 nm; TNT-Ta5: 20 nm; TNT-Ta7 <5 nm) were successfully fabricated by magnetron sputtering parameters given in Table 1.

In order to detect the surface elemental and binding compositions, XPS analysis was performed, as shown in Fig. 3A and C. The electronic orbitals of Ta 4p, Ta 4d, and Ta 4f were observed in tantalum-modified samples corresponding to the binding energies of 405, 230, and 25 eV. Meanwhile, compared with TNT, the binding energies of Ti 2p were decreased in the tantalum-modified samples, indicating the success of tantalum deposition and that the tantalum nanocoating was thicker with the increase of the sputtering duration. The detailed scan data in Fig. 3C showed that tantalum element was composed of Ta_2O_5 (+5), metallic Ta, and suboxides with low valence (+1 to +4). Moreover, Ta_2O_5 (+5) was prominent in all tantalum-modified samples, which was mainly attributed to the oxidation.[40]

In addition, the hydrophilic property and crystalline phase structure also affect the surface physical property.[41] Fig. 3C showed that the TNT surface possessed high hydrophilic property (5 ± 2.33°) compared with pure Ti (65 ± 2.67°), which was consistent with our previous studies.[28] The contact angle decreased 92% compared to that of pure Ti. This reason was complex, which might be related to the reaction products containing hydroxide compounds on the TNT surfaces, the introduction of oxygen elements, the nanotube arrays that provided space for liquid penetration, and the alteration of surface roughness.[42,43] According to previous studies, the nanotube arrays that provide the liquid to penetrate might be the prominent reason for the decrease of the contact angle.[40] The TNTs substrates in our study showed porous structure with large diameter (Fig. 1A and C), containing more water molecules and reducing the water contact angle. Notwithstanding, the nanotube arrays with larger diameter could provide more

Table 2 Real-time polymerase chain reaction primers of osteogenesis-related genes

Target genes	Primers
Runx2	Forward 5′-CCACAAGGACAGAGTCAGATTACA-3′
	Reverse 5′-TGGCTCAGATAGGAGGGGTA-3′
ALP	Forward 5′-GGCCAGCTACACCACAACA-3′
	Reverse 5′-CTGAGCGTTGGTGTTATATGTCTT-3′
COL-1	Forward 5′-CCTGAGCCAGCAGATTGA-3′
	Reverse 5′-TCCGCTCTTCCAGTCAG-3′
OPN	Forward 5′-CCCGGTGAAAGTGACTGATT-3′
	Reverse 5′-TTCTTCAGAGGACACAGCATTC-3′
OCN	Forward 5′-AGACTCCGGCGCTACCTT-3′
	Reverse 5′-CTCGTCACAAGCAGGGTTAAG-3′
GAPDH	Forward 5′-GGCATTGCTCTCAATGACAA-3′
	Reverse 5′-TGTGAGGGAGATGCTCAGTG -3′

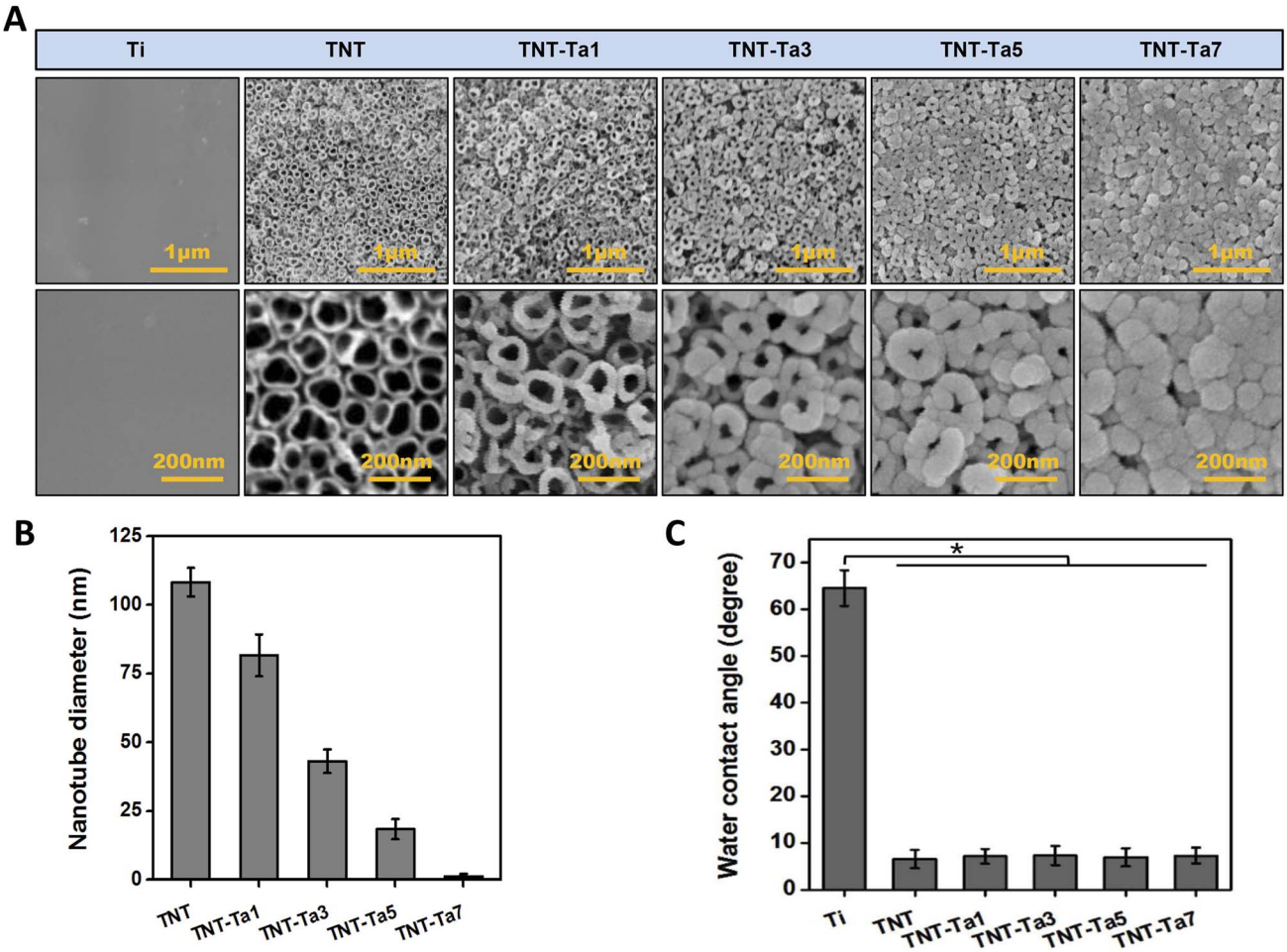

Fig. 1 (A) The SEM image of different specimens (Ti, TNT, TNT-Ta1, TNT-Ta3, TNT-Ta5, and TNT-Ta7) ($n = 6$). (B) Corresponding statistical analysis of the diameters of different nanotubes. (C) Water contact angle measurements of different specimens (Ti, TNT, TNT-Ta 1, TNT-Ta3, TNT-Ta5, and TNT-Ta7) ($n = 6$), *$p < 0.05$.

penetration space and thus create a more hydrophilic surface. Consistent with a previous study that the nanocoating significantly increased the water contact angle of TNTs,[28] the water contact angle of TNT-Ta1, TNT-Ta3, TNT-Ta5, and TNT-Ta7 was almost the same as that of TNTs (TNT-Ta1: 5.6 ± 2.38°, TNT-Ta3: 6.8 ± 5.28°, TNT-Ta5: 5.9 ± 6.78°, TNT-Ta7: 6.6 ± 7.83°). However, the reasons are not yet fully elucidated and we will be able to clarify it in our further experiment. The increase in the surface roughness and the alternation of surface topography might influence the result.[44,45]

The XRD patterns of the produced specimens were presented in Fig. 3C. It exhibited the characteristic peaks of Ti (JCPDS: 44-12-94), which was consistent with our previous study.[28] The main diffraction peaks of XRD were the characteristic peaks of titanium: 35.03°, 38.37°, 40.17°, 53.02°, 63.94°, 70.65°, 76.25°, and 77.33° (card number JCPDS: 44-12-94). On the other hand, the TiO_2 diffraction peaks (card number JCPDS: 21-1272) 25.2°, 37.8°, and 48° emerged after anodization, which proved the composition of TNTs. From these results, no obvious Ta signal can be detected by XRD evaluation, indicating that the deposition of the tantalum nanocoating could not change the crystalline phase structure. The reason may be attributed to the thinness of the tantalum coating, indicating that the magnetron sputtering technique was insufficient to produce the Ta crystal phase.[46] The surface roughness was compared in Fig. 2. Merely depending on the Sa value to compare the surface roughness was inadequate, which reflected the arithmetic average deviations of the profile height from the mean surface. Therefore, the parameter Sq was taken to indicate the root mean square average of the profile height deviations from the mean surface, which could react to the maximum heights and depths of the profile sensitively.[47,48] Fig. 2 showed that pure Ti possessed minimum roughness (Sa: 34 nm, Sq: 44.8 nm), while the anodization treatment increased the surface roughness significantly (Sa: 69.8 nm, Sq: 87.5 nm). Moreover, the deposition of the tantalum nanocoating also remarkably increased the surface roughness, and TNT-Ta7 (Sa: 199.6 nm, Sq: 221 nm) was the roughest substrate. The Sa/Sq values of all the substrates were ranked in the order Ti < TNT < TNT-Ta1 < TNT-Ta3 < TNT-Ta5 < TNT-Ta7, indicating that the surface roughness increased on prolonging the sputtering duration.

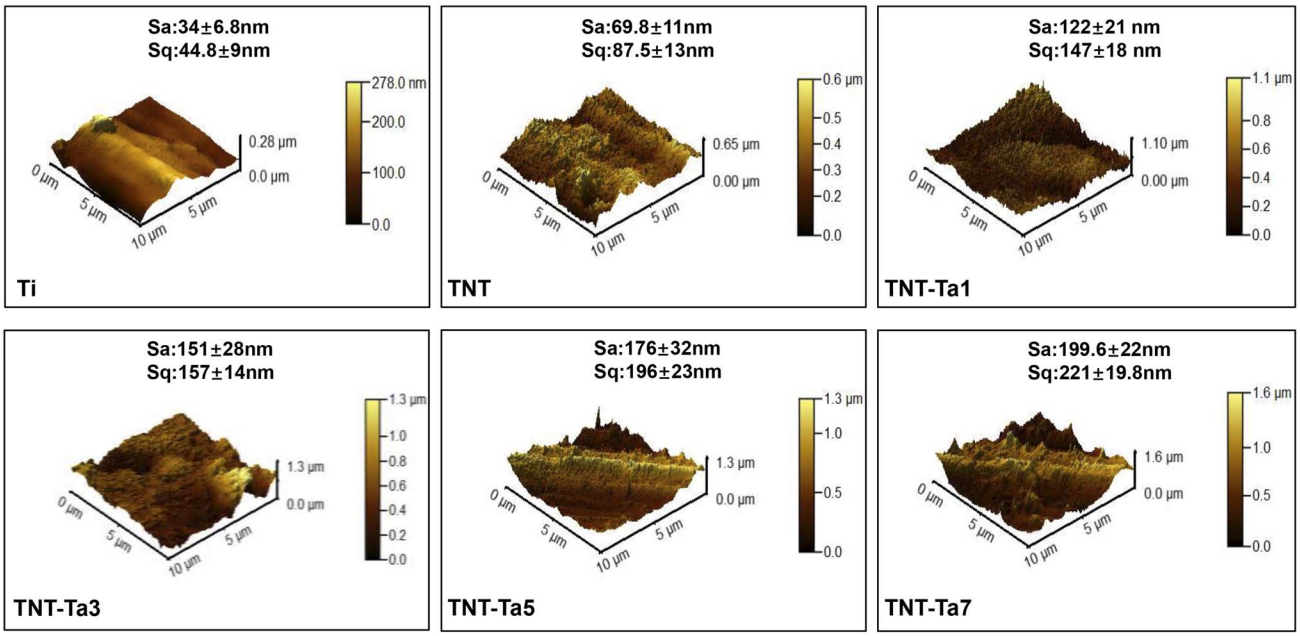

Fig. 2 AFM images showing the average roughness (Sa) and root mean square deviation of the surface (Sq) of different substrates ($n = 6$).

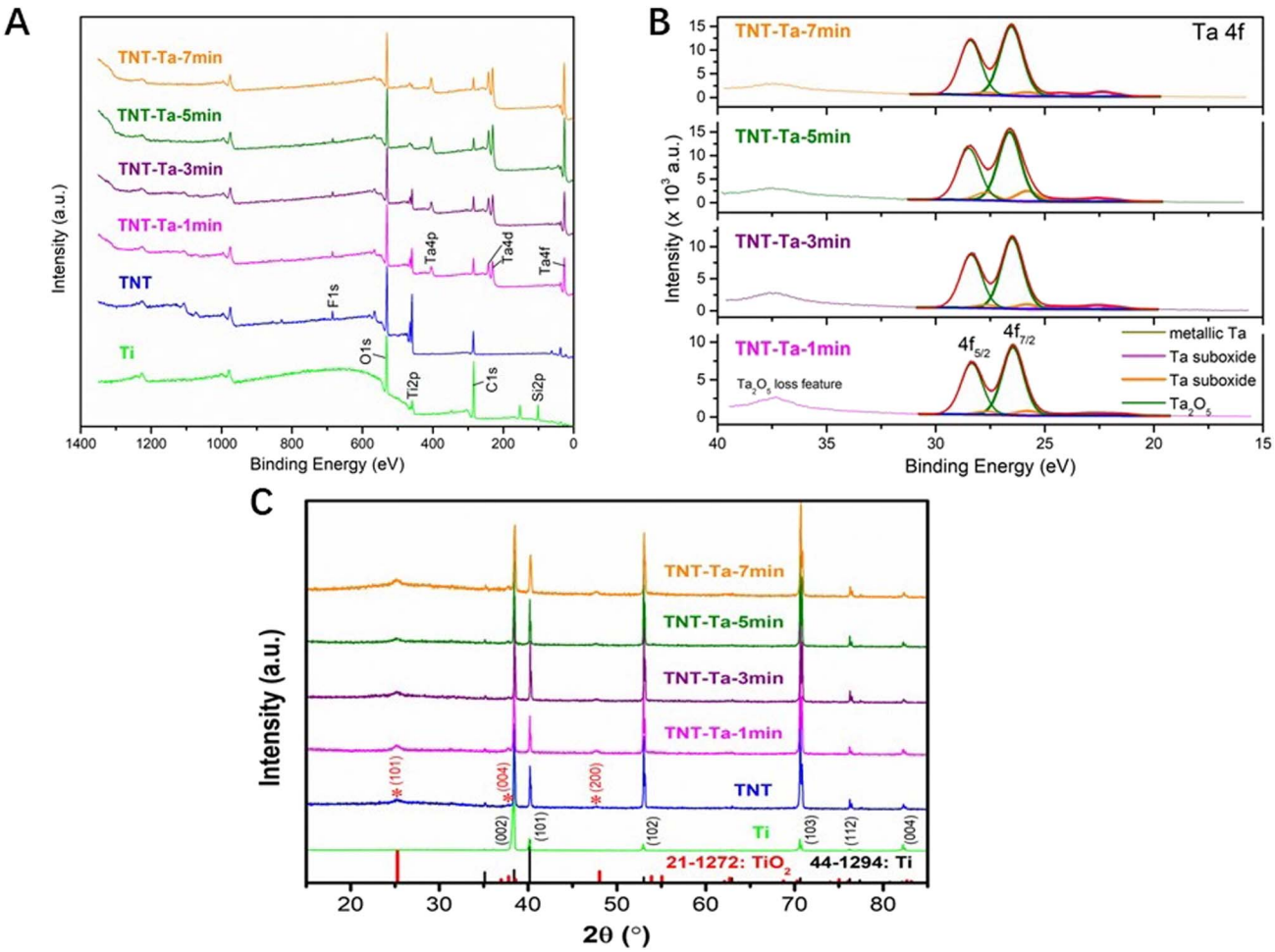

Fig. 3 (A) XPS analysis of different samples ($n = 6$), (B) detailed spectrum for Ta XPS analysis ($n = 6$). (C) XRD showing the crystalline structure of different samples (Ti, TNT, TNT-Ta 1, TNT-Ta3, TNT-Ta5, and TNT-Ta7) ($n = 6$).

3.2 *In vitro* cell experiment

3.2.1 MC3T3-E1 cell early adhesion. Cell adhesion influenced cell proliferation and differentiation significantly, which was the first step in successful bone-to-implant osteointegration.[49] The cell adhesion evaluation results were depicted in Fig. 4A and B after 0.5 h and 2 h of cell culture. Compared with the Ti group, the early cell adhesion on the TNT group was decreased both in 0.5 h and 2 h. However, the deposition of the tantalum nanocoating increased the cell adhesion gradually (TNT < TNT-Ta1< TNT-Ta3 < TNT-Ta5 < TNT-Ta7). In particular, the cell adhesion on TNT-Ta5 and TNT-Ta7 (TNT-Ta5:112 ± 13; TNT-Ta7: 118 ± 15) increased statistically compared with TNT and TNT-Ta1 (TNT: 82 ± 13; TNT-Ta1: 87 ± 11). Also, the cell adhesion in 2 h showed the same trend as that in 0.5 h. Compared with the TNT group (123 ± 12), the TNT-Ta3, TNT-Ta5, and TNT-Ta7 showed higher cell adhesion (TNT-Ta3:161 ± 16; TNT-Ta5: 182 ± 18; TNT-Ta7: 195 ± 13). Therefore, the tantalum nanolayer could increase the surface cell adhesion significantly, and TNT-Ta5 and TNT-Ta7 possessed the best cell adhesion property.

3.2.2 Cell morphology. The cell morphology was displayed in Fig. 5A, and the corresponding statistical analysis was depicted in Fig. 5B and C. After 6 h of cell incubation, the cells on the TNT, TNT-Ta1, and TNT-Ta3 showed shrunken cell body compared with Ti, TNT-Ta5, and TNT-Ta7. Moreover, after being incubated for 24 h, the cell morphology showed the same trend and the discrepancy seemed more obvious. The cells on TNT-Ta5 and TNT-Ta7 showed more patulous cell area compared with TNT and TNT-Ta1 after 24 h of cell culture. However, there was no significant difference between Ti, TNT-Ta5, and TNT-Ta7. In addition, compared with Ti and TNT, more filamentous pseudopodia could be observed on TNT-Ta3, TNT-Ta5, and TNT-Ta7 samples (Fig. 5A). In particular, TNT-Ta5 and TNT-Ta7 showed a large number of filamentous and actin microfilaments. Previous studies have proved that both the F-actin cytoskeleton network and filamentous pseudopodia were pivotal for cell morphology and cell proliferation.[50] Furthermore, the reason that the Ti surface was beneficial for the cell spreading area may be attributed to the smooth surface with no impurities, which was consistent with a previous study.[51] In addition, TNT-Ta1, TNT-Ta3, and TNT-Ta5 showed rounder cell

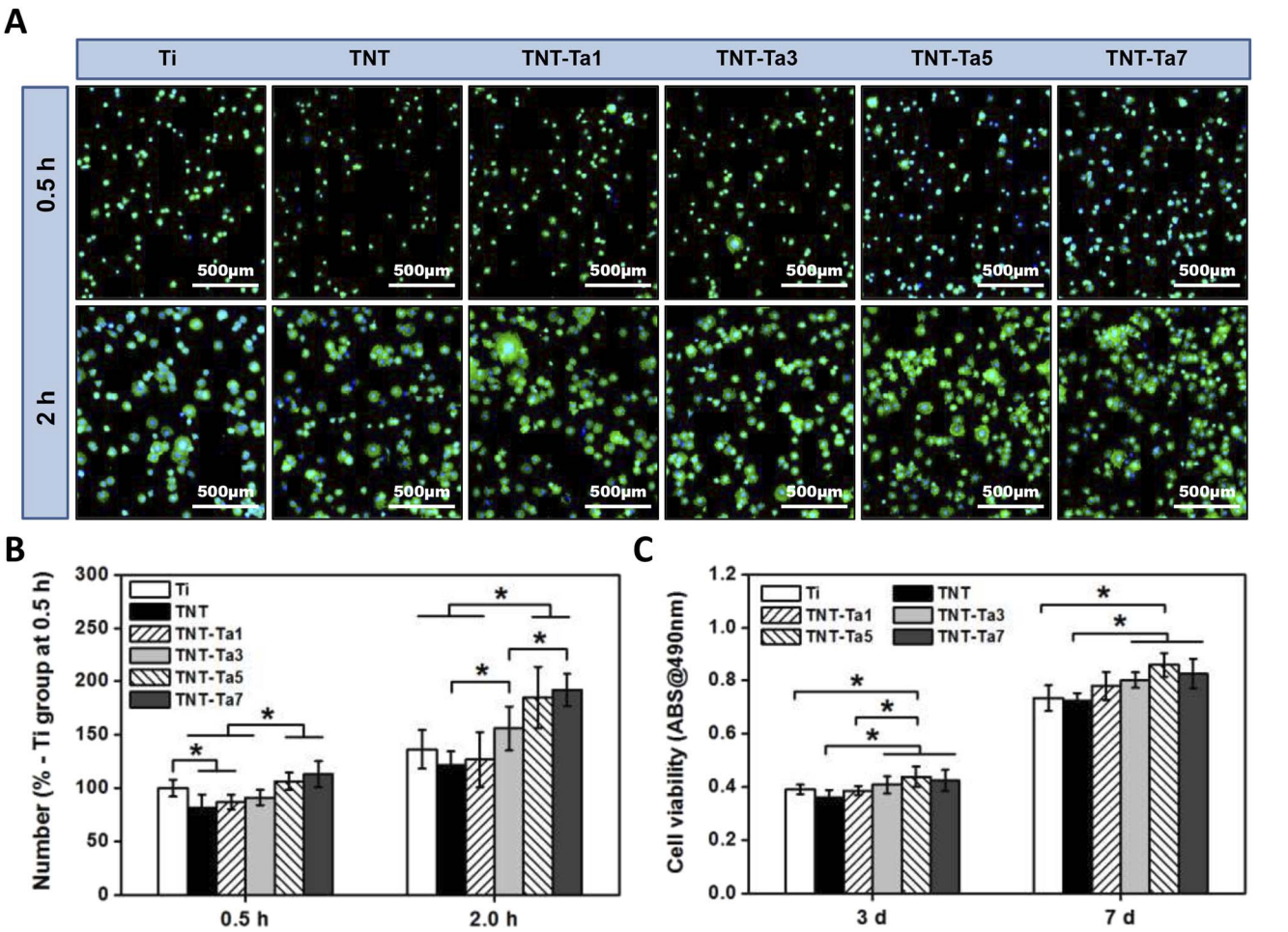

Fig. 4 (A) Fluorescent images of MC3T3-E1 cells adhesion on different samples (Ti, TNT, TNT-Ta1, TNT-Ta3, TNT-Ta5, and TNT-Ta7) after 0.5/2 h of cell seeding ($n = 6$). (B) Cell number counting of cell adhesion on different specimens ($n = 6$). (C) The proliferation of MC3T3-E1 cells on different samples (Ti, TNT, TNT-Ta 1, TNT-Ta3, TNT-Ta5, and TNT-Ta7) at 3/7 d ($n = 6$).

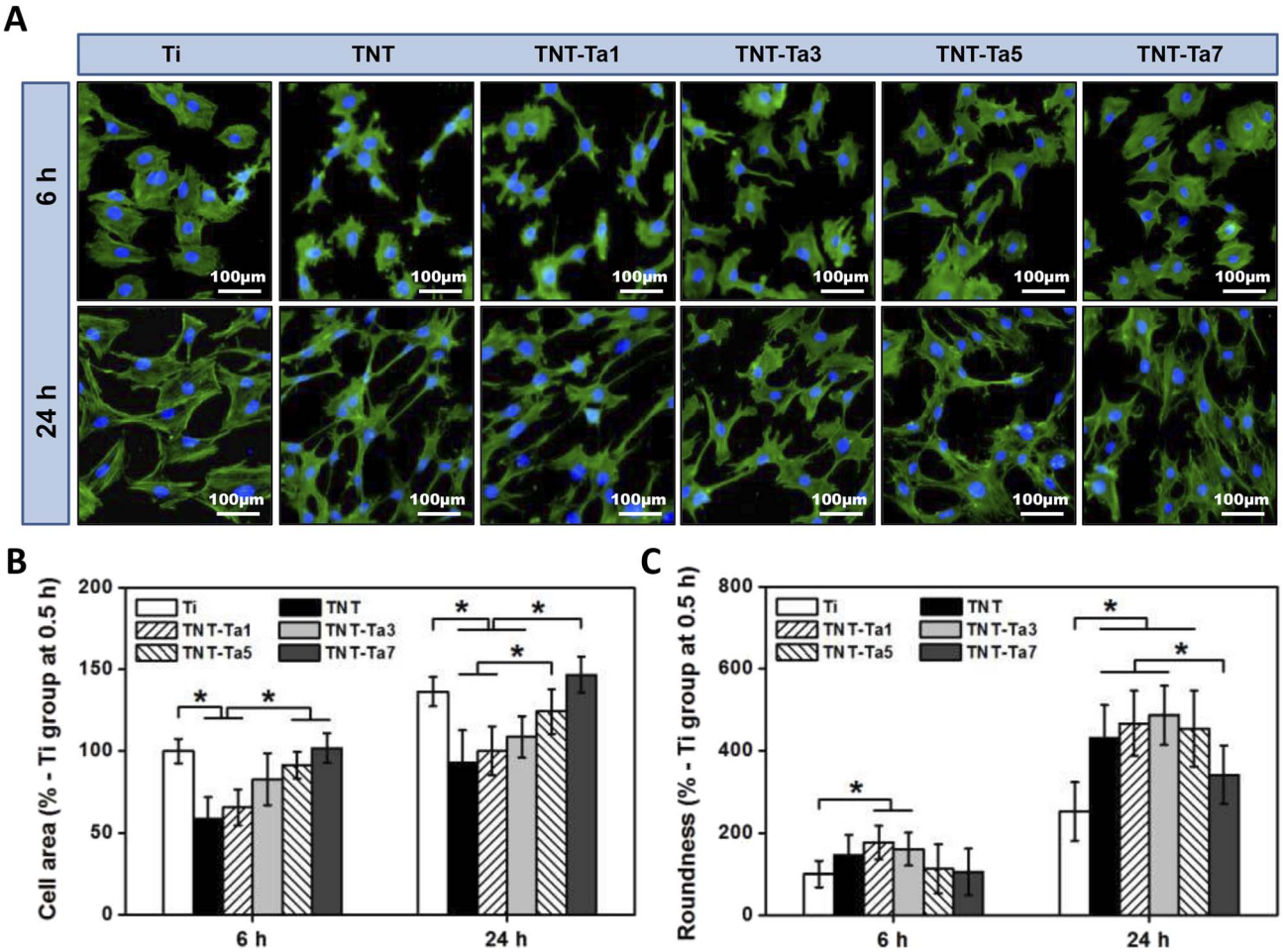

Fig. 5 (A) Fluorescent images of the cell morphology of MC3T3-E1 cells on different samples (Ti, TNT, TNT-Ta1, TNT-Ta3, TNT-Ta5, and TNT-Ta7) after 6/24 h of cell culture incubation ($n = 6$). (B) Statistical analysis of the cell area of different samples after 24 h of cell culture. (C) The statistical analysis of cell roundness of different samples after 24 h of cell culture incubation.

body than Ti ($P < 0.05$), which was mainly attributed to the tantalum function and the surface structure.[52,53] These results indicated that the tantalum nanocoating could promote the cell morphology, which might further influence pro-osteogenic property and osteogenic differentiation.

3.2.3 Cell viability. In order to evaluate the cell viability of MC3T3-E1 on different substrates, the MTT assay was conducted. As shown in Fig. 4C, the cell viability of the TNT group was decreased compared with the Ti group both after 3 d and 7 d of cell incubation, while the deposition of the tantalum nanolayer increased the cell viability. Pro-osteoblast cultured on TNT-Ta3, TNT-Ta5, and TNT-Ta7 substrates possessed significantly higher ($p < 0.05$) cell viability, compared with those cultured on TNT substrates. In addition, it seemed that TNT-Ta5 promoted the cell viability to the largest extend while it was decreased in the TNT-Ta7 group, indicating that the cytocompatibility of the tantalum nanocoating and TNT-Ta5 was the most suitable group for cell proliferation. The results might be attributed to the tantalum function, which showed beneficial effects on biocompatibility. Unlike the cell adhesion and cell morphology results, TNT-Ta5 showed the best cell viability both after 3/7 d of cell culture. On the one hand, the decrease in the nanotube diameter could increase the cell proliferation, and the size of 15–20 nm could achieve the best cell proliferation level by protein migration and attachment.[38,54] On the other hand, pro-osteoblast interacted with integrin protein after early adhesion, and small-sized nanotube substrate was conducive to integrin attachment site for pro-osteoblast. These results indicated that a narrow outer diameter of the nanotube and appropriate tantalum nanocoating endowed the TNT-Ta5 with the best cell proliferation capacity.

3.2.4 MC3T3-E1 cell differentiation. ALP activity, an early indicator of osteogenic differentiation, was applied to evaluate the osteogenic property of different substrates.[55] The results were displayed in Fig. 6A. Pro-osteoblast cells cultured on TNT and TNT-Ta specimens showed statistically increased ALP activity ($p < 0.05$) when compared with that on Ti group after 3 and 7 days of culture. Moreover, the ALP activity of TNT, TNT-Ta1, and TNT-Ta3 was higher ($p < 0.05$) than that of the Ti group after 7 d of osteogenic incubation. It indicated that the nanotube structures enhanced the osteogenic property of pro-osteoblasts, which was consistent with a previous study.[56]

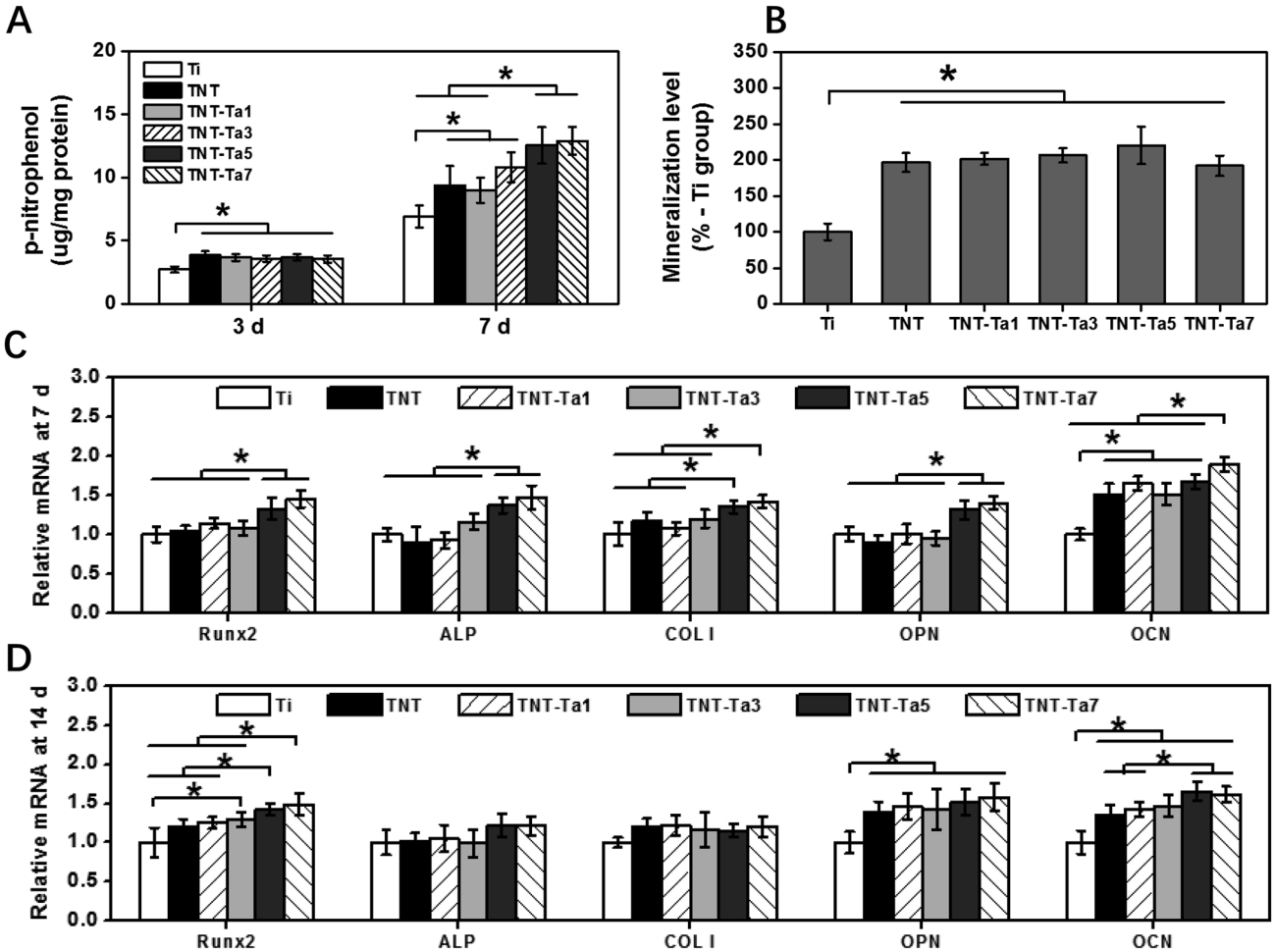

Fig. 6 (A) ALP activity of MC3T3-E1 on different samples after 3/7 d of osteogenic induction ($n = 6$). (B) Mineralization of MC3T3-E1 on different samples after 14 d of osteogenic induction ($n = 6$). (C) RT-qPCR analysis of osteogenesis-related genes of MC3T3-E1 on different samples after 7 d of osteogenic induction. (D) RT-qPCR analysis of osteogenesis-related genes of MC3T3-E1 on different samples after 7 d of osteogenic induction. *$p < 0.05$.

Moreover, pro-osteoblasts incubated on TNT-Ta5 and TNT-Ta7 possessed significantly higher ($p < 0.05$) ALP activity than those that grew on the Ti, TNT, and TNT-Ta1 specimens after 7 days of incubation, indicating the osteogenic induction of tantalum nanocoating. Therefore, tantalum nanocoating could enhance the ALP activity and further provide an alkaline microenvironment for mineralization.

In order to further access the osteogenic property of different specimens, alizarin red staining was evaluated to access the mineralization level. As shown in Fig. 6B, pro-osteoblasts cultured on TNT (196 ± 13%) and TNT-Ta specimens showed significantly enhanced ($P < 0.05$) mineralization compared with Ti (100 ± 11%), which might explain that tantalum nanocoating played a pivotal role in the mature stage of osteogenic differentiation.[57] Among the TNT-Ta specimens, the TNT-Ta5 group showed the highest mineralization level (220 ± 26%), indicating the osteogenic promotion property of suitable tantalum nanocoating and corresponding to previous studies.[40,58] On the one hand, tantalum promoted the proliferation and adhesion of pro-osteoblasts and enhanced the mineralization level by the Wnt/β-catenin and TGF-β/smad signal pathway.[59] On the other hand, tantalum could activate the MAPK/ERK signaling pathway and thus promote osteogenesis-related gene expression.[45] Except for the tantalum function, the decreased nanotube diameter of TNTs also plays an important role in osteogenic promotion. A previous study proved the TNTs with smaller diameter (<30 nm) showed enhanced ALP activity and ECM mineralization, while TNTs with large diameter exhibited a negative effect on cell growth.[17] Additionally, previous studies also proved that TiO_2 with pore diameter of 20 nm promoted osteogenic induction, while osteoblastic maturation promotion was observed on surfaces with a pore diameter of 50 nm.[37] As a result, the surface structure properties, including surface roughness and topography, could not only influence the physical properties, such as wettability and energy, but also the biological behavior. For instance, a previous study had proved that highly rough pure titanium coating promoted the osteogenic differentiation.[60] It also indicated that surfaces with a higher roughness were beneficial for the expression of osteogenesis-related genes, while surfaces with lower roughness

of 15 nm were conducive to chondrogenic gene expression.[61] Therefore, the biological response of objective surfaces was affected by the combination of surface properties including wettability, surface roughness, and surface topography.

In order to evaluate the osteogenic property at a genetic level, the RT-qPCR experiment was conducted. After 7 days of cell culture, the expression of Runx2, ALP, OPN, OCN, and COL-1 on the TNT-Tpa5 and TNT-Ta7 group was statistically higher than those on the control group ($P < 0.05$). Unlike 7 d of cell culture, the RT-qPCR results at 14 d showed that both the TNT-Ta5 and TNT-Ta7 group promoted the expression of Runx2, OPN, and OCN significantly ($P < 0.05$) when compared with Ti and TNT. Among these osteogenesis-related genes, Runx2 was regarded as an important transcription factor of osteogenic induction and bone to implant osteointegration.[62] Meanwhile, the TNT-Ta5 group (1.33 ± 0.13/1.41 ± 0.075) showed significantly higher expression level of Runx2 than Ti (1.00 ± 0.09/1.00 ± 0.18), TNT (1.03 ± 0.07/1.19 ± 0.10), and TNT-Ta1 (1.14 ± 0.07/1.24 ± 0.07) both after 7/14 days of incubation. These results indicated that the tantalum nanocoating plays a pivotal role in osteogenesis-related gene expression (Runx2, ALP, OPN, OCN, and COL-1) and thus promoted the osteogenic property. It was corresponding to a previous study that porous tantalum scaffold could enhance the expression of osteogenesis-related gene (ALP, OSX, COL-1, OSN, and OCN) expression by the activation of the MAPK/ERK signaling pathway.[63] Furthermore, the TNT-Ta5 group was regarded as an ideal group with the best cytocompatibility and excellent osteogenic ability, indicating that the tantalum nanocoating with an appropriate thickness on TNTs could provide conducive cell condition.[64] Moreover, the phenomenon that ALP gene expression was decreased after 14 days of cell culture was consistent with a previous study, which was mainly attributed to the transfer to mineralization.[15] It indicated that the tantalum nanocoating promoted the gene expression of Runx2, ALP, OPN, OCN, and COL-1 at the early stage and thus enhanced the ALP activity and osteogenic induction. Afterward, the gene expression of Runx2, OPN, and OCN was further promoted at a later stage to further enhance the mineralization and osteogenic property.

3.2.5 Drug release. Due to the long-term healing process of the bone defect, a drug releasing implant with sustainable drug release is important. The drug release test was conducted to analyze the drug release property. Fig. 7A showed that the hydrophilic drug (vancomycin) was released quickly in the groups of TNT, TNT-Ta1, and TNT-Ta7, which were released in the largest amounts (75%) within 3 h and completely released within 12 h. Although the release curve of the TNT-Ta3 group was relatively slow compared with TNT and TNT-1, the drug was completely released within 24 h. Compared with other groups, the vancomycin in the TNT-Ta5 group was completely released

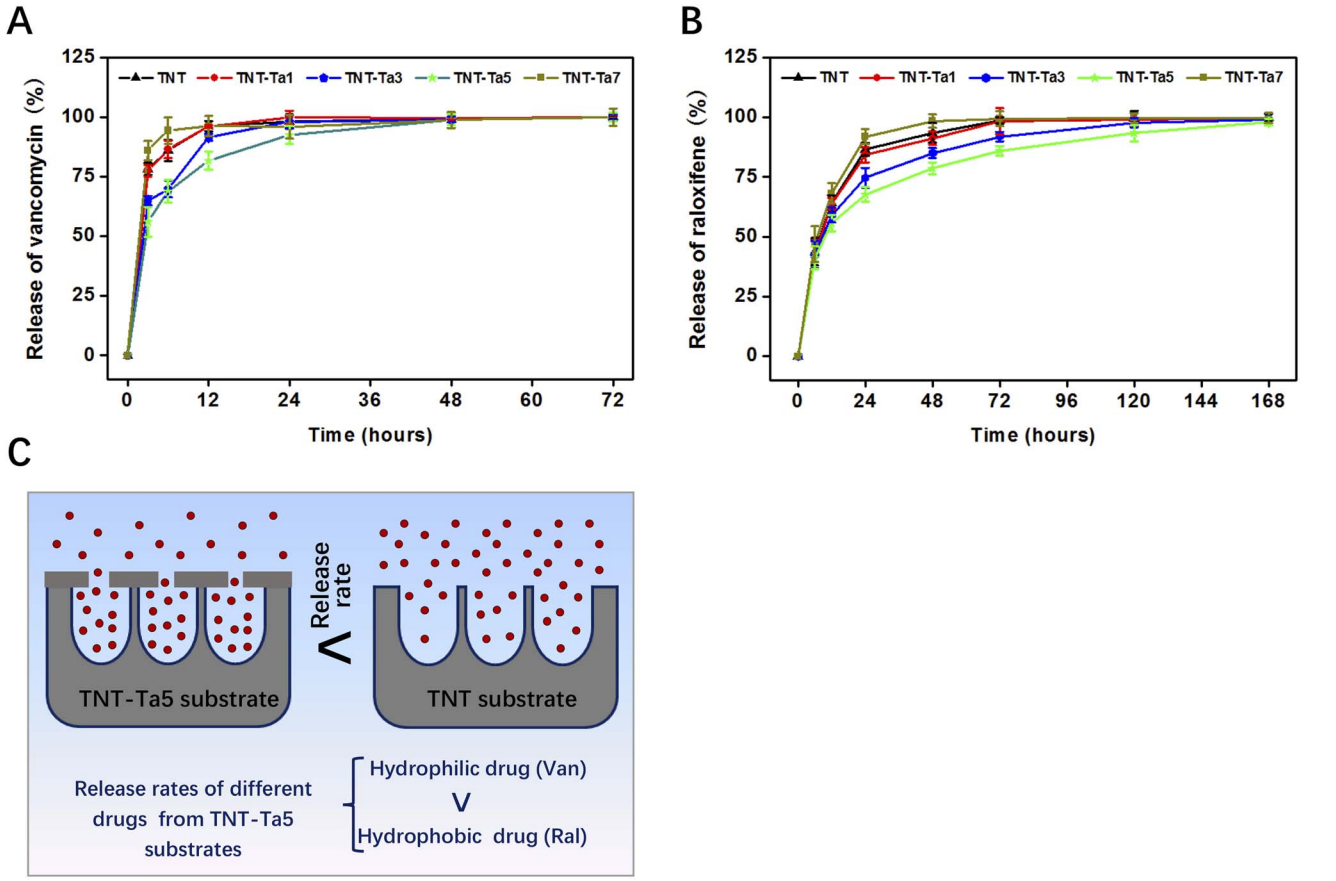

Fig. 7 (A) Drug release test of hydrophilic vancomycin. (B) Drug release test of hydrophobic raloxifene vancomycin. (C) The diagram of experimental design of this study.

after 48 h, showing the slowest drug release rate. It indicated that TNT-Ta5 was the best drug release system, while it was easy for the hydrophilic drug to be completely released. The accumulative release profiles of hydrophobic raloxifene are listed in Fig. 7A. The drug release of TNT-Ta7, TNT-Ta1, and TNT was fast and totally released after 72 h, while the release of TNT-Ta3 was significantly slow and released completely after 120 h. Interestingly, the release profiles of hydrophobic raloxifene in the TNT-Ta5 group showed the slowest drug release, which showed sustained release even at 168 h. The release results indicated that the TNT-Ta5 group possessed excellent drug release property. In this study, the tantalum nanocoating was applied to optimize the drug release property and the TNT-Ta5 group was selected as the most suitable drug release system. It possessed a tube diameter of 20 nm, which was narrowed by the tantalum nanocoating (Fig. 1A and B) and possessed sustained drug release property. Additionally, the rapid drug release in the TNT-Ta7 group was mainly attributed to the completely covered titanium nanotube, which impeded the drug absorption. The poor release property of the TNT and TNT-Ta1 groups was attributed to the large nanotube diameter, which was unable to block drug release. Compared with the hydrophilic drug (48 h), the hydrophobic drug (168 h) release in the TNT-Ta5 group possessed more sustained release effects. Therefore, it proved that the hydrophobic drug was more suitable for drug release in TNT-Ta5 than the hydrophilic drug. Above all, the TNT-Ta5 drug delivery system possessed sustained release property, excellent cytocompatibility, and osteogenic ability, which possessed potential application in implant design. Compared with drug release, the Ta release in this system could not be evaluated. According to the XPS results, Ta_2O_5 (+5) was prominent in all tantalum-modified samples, which was stable in body fluid, thus making it difficult to release the Ta ion.[47] Numerous techniques have been applied to cover the biomaterial with bioactive coatings. Methods like antimicrobial peptides (AMPs) or osteogenically-enhanced peptides coating showed effective biofunctions, while the quick drug release and the difficulties of sterilization impede the application.[65] Alternatively, coatings that were composed of synthetic or organic materials (*e.g.*, hydrogels, PLGA, chitosan, and polymers) immobilized on TNTs to produce drug delivery systems possessed sustained drug release property.[66–68] However, the lack of biocompatibility, poor coating binding strength, and difficulty of sterilization challenge the transformation and application.[69] Compared with chemical or biological coatings, the tantalum nanocoating used in this study possessed excellent biocompatibility, osteogenic property, and high binding strength.[70] Moreover, the simple modification procedure and effective sustained drug property make it valuable and transformative for application. The limitations of this tantalum nanocoating technique was the ineffective sustained release of the hydrophilic drug and the lack of animal experiments. Therefore, we will conduct animal experiments to further evaluate the biofunctionality *in vivo* and more techniques will be explored for optimization.

4. Conclusion

In this study, a new tantalum nanocoating modified drug release system was established by the combination of anodization and magnetron sputtering. This tantalum modified drug delivery system was expected to enhance the biological function and sustained drug release ability. In view of the relevant experimental results and analysis, the following conclusions could be summarized.

- The surface characterization results showed that the tantalum-modified drug delivery system was successfully prepared and tantalum element was present as Ta_2O_5.
- The *in vitro* cell experiment indicated that TNT-Ta5 and TNT-Ta7 possessed superior pro-osteogenic induction property, which upregulated OCN, Runx2, and OPN gene expression and thus enhanced the osteogenic differentiation.
- The drug release test indicated that the TNT-Ta5 group had the best sustained drug release property, especially for the hydrophobic drug (168 h).
- The suitable tantalum nano-coating on TNTs (TNT-Ta5) was confirmed as a promising strategy for implant design.

Conflicts of interest

The authors declare that they have no known competing financial interests or personal relationships that could have appeared to influence the work reported in this paper.

Acknowledgements

This work is supported by the National Natural Science Foundation of China (82071170), Traditional Chinese Medicine Science and Technology Program of Zhejiang Province (2023ZR109) and Wenzhou Public Welfare Science and Technology Project (Y2020209).

References

1 J. Liang, S. Xu, M. Shen, B. Cheng, Y. Li, X. Liu, D. Qin, A. Bellare and L. Kong, Osteogenic activity of titanium surfaces with hierarchical micro-/nano-structures obtained by hydrofluoric acid treatment, *Int. J. Nanomed.*, 2017, **12**, 1317.

2 H. Wang, Q. Xu, H. Hu, C. Shi, Z. Lin, H. Jiang, H. Dong and J. Guo, The fabrication and function of strontium-modified hierarchical micro/nano titanium implant, *Int. J. Nanomed.*, 2020, 8983–8998.

3 P. Jiang, Y. Zhang, R. Hu, B. Shi, L. Zhang, Q. Huang, Y. Yang, P. Tang and C. Lin, Advanced surface engineering of titanium materials for biomedical applications: From static modification to dynamic responsive regulation, *Bioact. Mater.*, 2023, **27**, 15–57.

4 S. Kligman, Z. Ren, C.-H. Chung, M. A. Perillo, Y.-C. Chang, H. Koo, Z. Zheng and C. Li, The impact of dental implant surface modifications on osseointegration and biofilm formation, *J. Clin. Med.*, 2021, **10**(8), 1641.

5 K. A. Kravanja and M. Finšgar, A review of techniques for the application of bioactive coatings on metal-based implants to achieve controlled release of active ingredients, *Mater. Des.*, 2022, 110653.
6 X. He, F.-X. Reichl, S. Milz, B. Michalke, X. Wu, C. M. Sprecher, Y. Yang, M. Gahlert, S. Röhling and H. Kniha, Titanium and zirconium release from titanium- and zirconia implants in mini pig maxillae and their toxicity in vitro, *Dent. Mater.*, 2020, **36**(3), 402–412.
7 A. Rezvan, E. Sharifikolouei, A. Lassnig, V. Soprunyuk, C. Gammer, F. Spieckermann, W. Schranz, Z. Najmi, A. Cochis and A. C. Scalia, Antibacterial activity, cytocompatibility, and thermomechanical stability of Ti40Zr10Cu36Pd14 bulk metallic glass, *Mater. Today Bio*, 2022, **16**, 100378.
8 J. C. Souza, M. B. Sordi, M. Kanazawa, S. Ravindran, B. Henriques, F. S. Silva, C. Aparicio and L. F. Cooper, Nano-scale modification of titanium implant surfaces to enhance osseointegration, *Acta Biomater.*, 2019, **94**, 112–131.
9 L. Sun, X. Chen, K. Ma, R. Chen, Y. Mao, R. Chao, H. Wang, B. Yu, J. Wang and S. Zhang, Novel Titanium Implant: a Three-dimensional Multifunction Architecture with Charge-trapping and Piezoelectric Self-stimulation, *Adv. Healthcare Mater.*, 2023, 2202620.
10 C. Tang, J. Deng, R. Xu, J. Li, C. Yin, Y. Yang, Y. Zhou and F. Deng, Micro/nano-modified Titanium Surfaces Accelerate Osseointegration *via* Rab7-dependent Mitophagy, *Biomater. Sci.*, 2023, **11**(2), 666–677.
11 J. Tang, L. Chen, D. Yan, Z. Shen, B. Wang, S. Weng, Z. Wu, Z. Xie, J. Shao and L. Yang, Surface functionalization with proanthocyanidins provides an anti-oxidant defense mechanism that improves the long-term stability and osteogenesis of titanium implants, *Int. J. Nanomed.*, 2020, 1643–1659.
12 N. Sarkar and S. Bose, Controlled delivery of curcumin and vitamin K2 from hydroxyapatite-coated titanium implant for enhanced *in vitro* chemoprevention, osteogenesis, and *in vivo* osseointegration, *ACS Appl. Mater. Interfaces*, 2020, **12**(12), 13644–13656.
13 D. Aggarwal, V. Kumar and S. Sharma, Drug-loaded biomaterials for orthopedic applications: A review, *J. Controlled Release*, 2022, **344**, 113–133.
14 S. Dai, L. Jiang, L. Liu, J. Chen, Y. Liao, S. He, J. Cui, X. Liu, A. Zhao and P. Yang, Photofunctionalized and drug-loaded TiO2 nanotubes with improved vascular biocompatibility as a potential material for polymer-free drug-eluting stents, *ACS Biomater. Sci. Eng.*, 2020, **6**(4), 2038–2049.
15 K. Zhang, Y. Zhu, X. Liu, Z. Cui, K. W. Yeung, H. Pan and S. Wu, Sr/ZnO doped titania nanotube array: an effective surface system with excellent osteoinductivity and self-antibacterial activity, *Mater. Des.*, 2017, **130**, 403–412.
16 L. Yuan, X. Xu, X. Song, L. Hong, Z. Zhang, J. Ma and X. Wang, Effect of bone-shaped nanotube-hydrogel drug delivery system for enhanced osseointegration, *Biomater. Adv.*, 2022, **137**, 212853.
17 K. Wang, H. Jin, Q. Song, J. Huo, J. Zhang and P. Li, Titanium dioxide nanotubes as drug carriers for infection control and osteogenesis of bone implants, *Drug Delivery Transl. Res.*, 2021, **11**(4), 1456–1474.
18 Y. Liu, C. Xie, F. Zhang and X. Xiao, pH-responsive TiO2 nanotube drug delivery system based on iron coordination, *J. Nanomater.*, 2019, 1–7.
19 T. Guo, K. Gulati, H. Arora, P. Han, B. Fournier and S. Ivanovski, Orchestrating soft tissue integration at the transmucosal region of titanium implants, *Acta Biomater.*, 2021, **124**, 33–49.
20 F. Wu, J. Xu, R. Yan, B. Hu, G. Li, M. Jin, X. Jiang, J. Li, P. Tang and J. Zhu, In vitro and *in vivo* evaluation of antibacterial activity of polyhexamethylene guanidine (PHMG)-loaded TiO2 nanotubes, *Biomed. Mater.*, 2020, **15**(4), 045016.
21 J. Wu, J. Huang, J. Yun, J. Yang, J. Yang, A. Fok and Y. Wang, Enzyme-directed biomineralization coating on TiO2 nanotubes and its positive effect on osteogenesis, *ACS Biomater. Sci. Eng.*, 2019, **5**(6), 2769–2777.
22 B. Tao, Y. Deng, L. Song, W. Ma, Y. Qian, C. Lin, Z. Yuan, L. Lu, M. Chen and X. Yang, BMP2-loaded titania nanotubes coating with pH-responsive multilayers for bacterial infections inhibition and osteogenic activity improvement, *Colloids Surf., B*, 2019, **177**, 242–252.
23 X. Ma, D. Zhao, Y. Xiang, Y. Hua, W. Zhao, Y. Cui and Z. Zhang, Layer-by-layer self-assembly and clinical application in orthopedics, *J. Mater. Sci. Technol.*, 2022, **147**, 241–268.
24 J. Zhou, M. A. Frank, Y. Yang, A. R. Boccaccini and S. Virtanen, A novel local drug delivery system: Superhydrophobic titanium oxide nanotube arrays serve as the drug reservoir and ultrasonication functions as the drug release trigger, *Mater. Sci. Eng. C*, 2018, **82**, 277–283.
25 M. Mesgari, A. H. Aalami and A. Sahebkar, Antimicrobial activities of chitosan/titanium dioxide composites as a biological nanolayer for food preservation: A review, *Int. J. Biol. Macromol.*, 2021, **176**, 530–539.
26 C. Mutalik, G. Okoro, D. I. Krisnawati, A. Jazidie, E. Q. Rahmawati, D. Rahayu, W.-T. Hsu and T.-R. Kuo, Copper sulfide with morphology-dependent photodynamic and photothermal antibacterial activities, *J. Colloid Interface Sci.*, 2022, **607**, 1825–1835.
27 T. Zhang, Y. Liu, F. Zhang and X. Xiao, Polylysine-modified titania nanotube arrays for local drug delivery, *Micro Nano Lett.*, 2018, **13**(1), 93–95.
28 L. Yao, A. M. Al-Bishari, J. Shen, Z. Wang, T. Liu, L. Sheng, G. Wu, L. Lu, L. Xu and J. Liu, Osseointegration and anti-infection of dental implant under osteoporotic conditions promoted by gallium oxide nano-layer coated titanium dioxide nanotube arrays, *Ceram. Int.*, 2023, **49**(14), 22961–22969.
29 H. Gao, J. Yang, X. Jin, X. Qu, F. Zhang, D. Zhang, H. Chen, H. Wei, S. Zhang and W. Jia, Porous tantalum scaffolds: Fabrication, structure, properties, and orthopedic applications, *Mater. Des.*, 2021, **210**, 110095.
30 X. Hu, S. Mei, F. Wang, J. Qian, D. Xie, J. Zhao, L. Yang, Z. Wu and J. Wei, Implantable PEKK/tantalum microparticles composite with improved surface performances for

regulating cell behaviors, promoting bone formation and osseointegration, *Bioact. Mater.*, 2021, **6**(4), 928–940.

31 K.-H. Cheon, C. Park, M.-H. Kang, I.-G. Kang, M.-K. Lee, H. Lee, H.-E. Kim, H.-D. Jung and T.-S. Jang, Construction of tantalum/poly (ether imide) coatings on magnesium implants with both corrosion protection and osseointegration properties, *Bioact. Mater.*, 2021, **6**(4), 1189–1200.

32 L. Li, L. Yao, L. Wu, Q. Ma, S. Lin, X. Shen, C. Huang and L. Sheng, The characteristic and osteogenic effect of a nanoporous coating of zirconia implant, *Ceram. Int.*, 2022, **48**(17), 24260–24267.

33 J. Wu, K. Ueda and T. Narushima, Fabrication of Ag and Ta co-doped amorphous calcium phosphate coating films by radiofrequency magnetron sputtering and their antibacterial activity, *Mater. Sci. Eng. C*, 2020, **109**, 110599.

34 Z. Ding, Y. Wang, Q. Zhou, Z. Ding, Y. Wu, Y. Zhu, W. Shi and Q. He, The preparation and properties of multilayer Cu-MTa2O5 composite coatings on Ti6Al4V for biomedical applications, *Nanomaterials*, 2019, **9**(10), 1498.

35 L. Xing, H. Zheng, Y. Cao and S. Che, Coordination polymer coated mesoporous silica nanoparticles for pH-responsive drug release, *Adv. Mater.*, 2012, **24**(48), 6433–6437.

36 L. Zhao, L. Liu, Z. Wu, Y. Zhang and P. K. Chu, Effects of micropitted/nanotubular titania topographies on bone mesenchymal stem cell osteogenic differentiation, *Biomaterials*, 2012, **33**(9), 2629–2641.

37 J. S. Khaw, C. R. Bowen and S. H. Cartmell, Effect of TiO2 nanotube pore diameter on human mesenchymal stem cells and human osteoblasts, *Nanomaterials*, 2020, **10**(11), 2117.

38 Y. Li, S. Wang, Y. Dong, P. Mu, Y. Yang, X. Liu, C. Lin and Q. Huang, Effect of size and crystalline phase of TiO2 nanotubes on cell behaviors: a high throughput study using gradient TiO2 nanotubes, *Bioact. Mater.*, 2020, **5**(4), 1062–1070.

39 M. J. Gupte, W. B. Swanson, J. Hu, X. Jin, H. Ma, Z. Zhang, Z. Liu, K. Feng, G. Feng and G. Xiao, Pore size directs bone marrow stromal cell fate and tissue regeneration in nanofibrous macroporous scaffolds by mediating vascularization, *Acta Biomater.*, 2018, **82**, 1–11.

40 Z. Cao, L. Li, L. Yang, L. Yao, H. Wang, X. Yu, X. Shen, L. Yao and G. Wu, Osteoinduction evaluation of fluorinated hydroxyapatite and tantalum composite coatings on magnesium alloys, *Front. Chem.*, 2021, **9**, 727356.

41 M. F. Kunrath, A. L. Vargas, P. Sesterheim, E. R. Teixeira and R. Hubler, Extension of hydrophilicity stability by reactive plasma treatment and wet storage on TiO2 nanotube surfaces for biomedical implant applications, *J. R. Soc., Interface*, 2020, **17**(170), 20200650.

42 C. Pan, T. Liu, Y. Yang, T. Liu, Z. Gong, Y. Wei, L. Quan, Z. Yang and S. Liu, Incorporation of Sr2+ and Ag nanoparticles into TiO2 nanotubes to synergistically enhance osteogenic and antibacterial activities for bone repair, *Mater. Des.*, 2020, **196**, 109086.

43 X. Yang, Q. Wang, Y. Zhang, H. He, S. Xiong, P. Chen, C. Li, L. Wang, G. Lu and Y. Xu, A dual-functional PEEK implant coating for anti-bacterial and accelerated osseointegration, *Colloids Surf., B*, 2023, **224**, 113196.

44 S. S. Nisar, S. Arun and H. C. Choe, Plasma electrolytic oxidation coatings on femtosecond laser-treated Ti-6Al-4V alloy for bio-implant use arrays, *Surf. Coat. Technol.*, 2023, **464**, 129553.

45 X. Dou, X. Wei, G. Liu, S. Wang, Y. Lv, J. Li, Z. Ma, G. Zheng, Y. Wang and M. Hu, Effect of porous tantalum on promoting the osteogenic differentiation of bone marrow mesenchymal stem cells *in vitro* through the MAPK/ERK signal pathway, *J. Orthop. Translat.*, 2019, **19**, 81–93.

46 L. Li, L. Yao, H. Wang, X. Shen, W. Lou, C. Huang and G. Wu, Magnetron sputtering of strontium nanolayer on zirconia implant to enhance osteogenesis, *Mater. Sci. Eng. C*, 2021, **127**, 112191.

47 S. Wu, X. Shen, M. Chen, K. H. R. Yie, Z. Zhou, M. A. Al-Baadani, K. Fang, A. M. Al-Bishari, Z. Deng, J. Liu and L. Yao, Multifunctional TaCu-nanotubes coated titanium for enhanced bacteriostatic, angiogenic and osteogenic properties, *Mater. Sci. Eng. C*, 2021, **120**, 111777.

48 G. Jin, H. Qin, H. Cao, S. Qian, Y. Zhao, X. Peng, X. Zhang, X. Liu and P. K. Chu, Synergistic effects of dual Zn/Ag ion implantation in osteogenic activity and antibacterial ability of titanium, *Biomaterials*, 2014, **35**(27), 7699–7713.

49 T. Lu, J. Wen, S. Qian, H. Cao, C. Ning, X. Pan, X. Jiang, X. Liu and P. K. Chu, Enhanced osteointegration on tantalum-implanted polyetheretherketone surface with bone-like elastic modulus, *Biomaterials*, 2015, **51**, 173–183.

50 W.-T. Hsieh, Y.-S. Liu, Y.-h. Lee, M. G. Rimando, K.-h. Lin and O. K. Lee, Matrix dimensionality and stiffness cooperatively regulate osteogenesis of mesenchymal stromal cells, *Acta Biomater.*, 2016, **32**, 210–222.

51 X. Shen, K. Fang, K. H. R. Yie, Z. Zhou, Y. Shen, S. Wu, Y. Zhu, Z. Deng, P. Ma and J. Ma, High proportion strontium-doped micro-arc oxidation coatings enhance early osseointegration of titanium in osteoporosis by anti-oxidative stress pathway, *Bioact. Mater.*, 2022, **10**, 405–419.

52 S. Bencharit, T. Morelli, S. Barros, J. T. Seagroves, S. Kim, N. Yu, K. Byrd, C. Brenes and S. Offenbacher, Comparing initial wound healing and osteogenesis of porous tantalum trabecular metal and titanium alloy materials, *J. Oral. Implantol.*, 2019, **45**(3), 173–180.

53 L. Wu, Y. Dong, L. Yao, C. Liu, A. M. Al-Bishari, K. H. R. Yie, H. Zhang, J. Liu and G. Wu, Nanoporous tantalum coated zirconia implant improves osseointegration, *Ceram. Int.*, 2020, **46**(11), 17437–17448.

54 T. Wang, Z. Weng, X. Liu, K. W. Yeung, H. Pan and S. Wu, Controlled release and biocompatibility of polymer/titania nanotube array system on titanium implants, *Bioact. Mater.*, 2017, **2**(1), 44–50.

55 M. Deng, S. G. Kumbar, L. S. Nair, A. L. Weikel, H. R. Allcock and C. T. Laurencin, Biomimetic structures: biological implications of dipeptide-substituted polyphosphazene–polyester blend nanofiber matrices for load-bearing bone regeneration, *Adv. Funct. Mater.*, 2011, **21**(14), 2641–2651.

56 Z. Wang, B. Li, Q. Cai, X. Li, Z. Yin, B. Li, Z. Li and W. Meng, Advances and Prospects in Antibacterial-Osteogenic

Multifunctional Dental Implant Surface, *Front. bioeng. biotechnol.*, 2022, **10**, 921338.

57 Y. Zhang, R. Luo, J. Tan, J. Wang, X. Lu, S. Qu, J. Weng and B. Feng, Osteoblast behaviors on titania nanotube and mesopore layers, *Regener. Biomater.*, 2017, **4**(2), 81–87.

58 X. Wang, B. Ning and X. Pei, Tantalum and its derivatives in orthopedic and dental implants: Osteogenesis and antibacterial properties, *Colloids Surf., B*, 2021, **208**, 112055.

59 H. Qian, T. Lei, Z. Ye, Y. Hu and P. Lei, From the performance to the essence: the biological mechanisms of how tantalum contributes to osteogenesis, *Biomed Res. Int.*, 2020, **2020**, 5162524.

60 A. Martín Vilardell, N. Cinca i Luis, N. Garcia Giralt, S. Dosta Parras, I. García Cano, X. Nogués Solán and J. M. Guilemany, Osteoblastic cell response on high-rough titanium coatings by cold spray, *J Mater Sci Mater Med.*, 2018, **29**, 2.

61 C. C. Wang, Y. Hsu, F. Su, S. Lu and T.-M. Lee, Effects of passivation treatments on titanium alloy with nanometric scale roughness and induced changes in fibroblast initial adhesion evaluated by a cytodetacher, *J Biomed Mater Res A*, 2009, **88**(2), 370–383.

62 X. Zhang, M. Yang, L. Lin, P. Chen, K. Ma, C. Zhou and Y. Ao, Runx2 overexpression enhances osteoblastic differentiation and mineralization in adipose-derived stem cells *in vitro* and *in vivo*, *Calcif. Tissue Int.*, 2006, **79**, 169–178.

63 C. Luo, C. Wang, X. Wu, X. Xie, C. Wang, C. Zhao, C. Zou, F. Lv, W. Huang and J. Liao, Influence of porous tantalum scaffold pore size on osteogenesis and osteointegration: a comprehensive study based on 3D-printing technology, *Mater. Sci. Eng. C*, 2021, **129**, 112382.

64 M. Zhang, Y. Xue, X. Huang, D. Ma, J. Gao, S. Yu, L. Zhu and Y. Wu, Cytocompatibility and osteogenic activity of Ta-Ti-O nanotubes anodically grown on Ti6Al4V alloy, *Appl. Surf. Sci.*, 2023, **614**, 156165.

65 E. D. Freitas, R. A. Bataglioli, J. Oshodi and M. M. Beppu, Antimicrobial peptides and their potential application in antiviral coating agents, *Colloids Surf., B*, 2022, 112693.

66 K. D. Jandt and D. C. Watts, Nanotechnology in dentistry: Present and future perspectives on dental nanomaterials, *Dent. Mater.*, 2020, **36**(11), 1365–1378.

67 M. F. Kunrath and M. M. Campos, Metallic-nanoparticle release systems for biomedical implant surfaces: Effectiveness and safety, *Nanotoxicology*, 2021, **15**(6), 721–739.

68 N. Poth, V. Seiffart, G. Gross, H. Menzel and W. Dempwolf, Biodegradable chitosan nanoparticle coatings on titanium for the delivery of BMP-2, *Biomolecules*, 2015, **5**(1), 3–19.

69 D. Ionita, D. Bajenaru-Georgescu, G. Totea, A. Mazare, P. Schmuki and I. Demetrescu, Activity of vancomycin release from bioinspired coatings of hydroxyapatite or TiO2 nanotubes, *Int. J. Pharm.*, 2017, **517**(1–2), 296–302.

70 M. F. Kunrath, F. A. Shah and C. Dahlin, Bench-to-bedside: Feasibility of nano-engineered and drug-delivery biomaterials for bone-anchored implants and periodontal applications, *Mater. Today Bio*, 2023, **18**, 100540.